Sigma Journal of Engineering and Natural Sciences
Web page info: https://sigma.yildiz.edu.tr
DOI: 10.14744/sigma.2023.00053

Journal of Engineering and Natural Sciences
Mühendislik ve Fen Bilimleri Dergisi

Research Article

A numerical method for an inverse problem concerning the two-dimensional diffusion equation with source control parameter by new polynomials

Saeid ABBASBANDY[1,*], Jalal HAJISHAFIEIHA[1]

[1]*Department of Applied Mathematics, Faculty of Sciences, Imam Khomeini International University, Qazvin, 34149-1681, Iran*

ARTICLE INFO

Article history
Received: 20 April 2021
Revised: 08 July 2021
Accepted: 28 September 2021

Keywords:
Inverse Problem; Time-Dependent Diffusion Coefficient; Over-Specification Condition; Nonlocal Boundary Condition; Chebyshev Polynomials

ABSTRACT

In this paper, we aim to find a control parameter in two-dimensional parabolic equations with the over-specification conditions. The present method is implemented on two problems with different over-specification conditions. This method produces new polynomials by combining Chebyshev polynomials and using an unknown parameter. The numerical solution of the problem is estimated by the linear combination of the new polynomials. By collocation method, the unknown coefficients of this linear combination and new unknown parameter are obtained by solving a nonlinear system by the least-squares method at each of the collocation points. Finally, with interpolation on all functions obtained at all collocation points, we will give an approximation solution. The results of this method are calculated for two types of interpolation points. The results obtained from the present method are better than the results of finite difference method.

Cite this article as: Abbasbandy S, Hajishafieiha J. A numerical method for an inverse problem concerning the two-dimensional diffusion equation with source control parameter by new polynomials. Sigma J Eng Nat Sci 2023;41(3):469–480.

INTRODUCTION

Most of the activities of engineering, science, and medicine are based on inverse problems. Among the fields in which inverse problems play a main role, the following branches can be pointed out: geophysics [1], optic [2], radar [3], acoustics [4], communication theory, signal processing [5], tomography, medical imaging [6]. There are two analytical and numerical methods for solving inverse problems. In this article, a new numerical method is suggested to solve a specific type of inverse problem. Several numerical methods are presented to solve the inverse problems that can be mentioned in the following methods: Bernstein Galerkin method [7], finite difference method [8], regularization method, mollification method [9], radial basis function method [10]. Due to the difficulty of solving inverse problems such as divergence in iterative methods or ill-posedness in methods that lead to the creation of system equations, it is important to present new methods that do not cause these problems.

In this paper, with the help of Chebyshev polynomials, we obtain a class of basic functions that approximates the

*__Corresponding author.__
*E-mail address: abbasbandy@ikiu.ac.ir; abbasbandy@yahoo.com
This paper was recommended for publication in revised form by Amin Shahsavar

solution of the inverse problem. The inverse problem discussed in this paper is a two-dimensional inverse problem in which the source parameter is unknown. This inverse problem has been solved in [11] and [12] by the finite difference method. Very recently in a one-dimensional case, this problem has been solved by the same authors in [13]. Here, we will consider two cases.

Problem 1) We will find a pair of functions $w(x, y, t)$, $P(t)$ in the following equation

$$w_t - w_{xx} - w_{yy} = P(t)w + f(x,y,t), \quad (x,y,t) \in \Omega = [0,1]^2 \times [0,T], \qquad (1)$$

with the following initial

$$w(x,y,0) = \psi(x,y), \quad (x,y) \in [0,1]^2,$$

and boundary conditions

$$\begin{aligned} w(0,y,t) &= k_0(y,t), \quad (y,t) \in \Omega_1, \\ w(1,y,t) &= k_1(y,t), \quad (y,t) \in \Omega_1, \\ w(x,0,t) &= l_0(x,t), \quad (x,t) \in \Omega_1, \\ w(x,1,t) &= l_1(x,t), \quad (x,t) \in \Omega_1, \end{aligned}$$

where $\Omega_1 = [0,1] \times [0,T]$ and

$$\int_0^1 \int_0^1 w(x,y,t)\,dxdy = E(t), \quad t \in [0,T].$$

Let ψ, k_0, k_1, l_0, l_1 and f are known functions and w, P are unknown functions. To determine the existence, uniqueness and stability of the solution, we refer to [14].

Problem 2) Like previous problem, we will consider

$$w_t - w_{xx} - w_{yy} = P(t)w + f(x,y,t), \quad (x,y,t) \in \Omega, \qquad (2)$$

with the following initial condition

$$w(x,y,0) = \psi(x,y), \quad (x,y) \in [0,1]^2,$$

and boundary conditions

$$\begin{aligned} w(0,y,t) &= k_0(y,t), \quad (y,t) \in \Omega_1, \\ w(1,y,t) &= k_1(y,t), \quad (y,t) \in \Omega_1, \\ w(x,0,t) &= l_0(x,t), \quad (x,t) \in \Omega_1, \\ w(x,1,t) &= l_1(x,t), \quad (x,t) \in \Omega_1, \end{aligned}$$

with a condition at a point (x_0, y_0) like

$$w(x_0,y_0,t) = E(t), \quad (x_0,y_0) \in [0,1]^2, \quad t \in [0,T],$$

where ψ, k_0, k_1, l_0, l_1 and f are known functions and w, P are unknown functions. To determine the existence, uniqueness and stability of the solution, we refer to [15].

Existence, Uniqueness, and Stability of the Solution

Suppose that

$$\begin{aligned} & w_t = Lu + P(t)w + f(x,y,t), \quad Q_T = \left\{(x,y,t) : (x,y) \in [0,1]^2, t \in [0,T]\right\}, \\ & w(x,y,0) = \psi(x,y), \qquad (x,y) \in [0,1]^2, \\ & w(x,y,t) = \chi(x,y,t), \qquad (x,y) \in \partial[0,1]^2 \times (0,T), \\ & \int_0^1\int_0^1 w(x,y,t)\,dxdy = E(t), \qquad t \in [0,T]. \end{aligned}$$

Which in problem 2, the following condition replaces the above condition in problem 1

$$w(x_0,y_0,t) \aleph E(t), \quad (x_0,y_0) \quad [0,1]^2, t \quad [0,T],$$

where the linear operator L is

$$Lw = \sum_{i,j=1}^{n} (a_{ij}(x,y,t) w_{x_i})_{x_j}.$$

Theorem 1.1: In view of the above assumptions, the inverse problems 1 and 2 have a unique solution and the solution depends continuously upon the data.

Proof: See [15].

To solve the problem, we use the following transformation:

$$u(x,y,t) = w(x,y,t)\exp\{-\int_0^t P(\xi)d\xi\}, \qquad (3)$$

$$\begin{aligned} & r(t) = \exp\{-\int_0^t P(\xi)d\xi\}, \\ & w = w(x,y,t) = u(x,y,t)\exp\{\int_0^t P(\xi)d\xi\}, \end{aligned}$$

we have

$$\begin{aligned} & u_t = Lu + r(t)f(x,y,t), \\ & u(x,y,0) = \psi(x,y), \qquad (x,y) \in [0,1]^2, \\ & u(x,y,t) \aleph \chi(x,y,t)r(t), \quad (x,y) \quad [0,1]^2 \quad [0,T], \qquad (4) \\ & r(t) = \frac{u(x_0,y_0,t)}{E(t)}, \qquad t \in [0,T]. \end{aligned}$$

In Section 2, the definitions and propositions needed in the next sections are brought. In Section 3, the present numerical method is described. Section 4 includes convergence and stability theorems and proof of them. In Section 5, examples and numerical results and tables and figures related to examples are displayed. Section 6 is the overall conclusion of the present article.

Polynomial functions

In mathematics, especially in applied mathematics, polynomials have always played a main role in the approximation theory [16,17]. In this paper, polynomials with a parameter a are used that this parameter is optimized in calculations.

Definition [18]: Assume a is a constant parameter. New polynomials are produced as follows

$$A_0(x) = 1,$$
$$A_n(x) \aleph ax U_{n-1}(x) \quad U_n(x), \quad n \quad 1,$$

where U_n is the second kind Chebyshev polynomial.

The following equations are also established:

$$A_{n+1}(t) = 2tA_n(t) \quad A_{n-1}(t), \; n \quad 1, \tag{5}$$

$$A_n(t) = (1+\frac{a}{2})U_n(t) + \frac{a}{2}U_{n-2}(t), \quad n \geq 2, \tag{6}$$

there are many propositions about these polynomials in [18] and a new application by the same authors in [13,20].

Proposition 2.1: U_n is the eigenfunction of the singular Sturm-Liouville problem:

$$[(1-t^2)^{-1/2}\frac{d}{dt}((1-t^2)^{3/2}\frac{d}{dt}) + n(n+2)]U_n(t) = 0, \tag{7}$$

for $n = 0,1,2,\ldots$.

Proposition 2.2: Assume that $\omega(t) = \sqrt{1-t^2}$, then

$$\left(U_n, U_m\right)_\omega = \int_{-1}^{1} U_n(t)U_m(t)\omega(t)dt = \frac{\pi}{2}\delta_{n,m}, \tag{8}$$

$$\int_{-1}^{1} \frac{dU_n(t)}{dt}\frac{dU_m(t)}{dt}\omega^3(t)dt = \frac{1}{2}n(n+2)\delta_{n,m}. \tag{9}$$

Remark 2.1:

$$\int_{-1}^{1} \omega^3(t)\frac{dU_n(t)}{dt}dt = 0, \tag{10}$$

$$\int_{-1}^{1} \omega^3(t)U_n(t)dt = 0. \tag{11}$$

Numerical Solution Method

In the present method, the first, the time interval is discrete. At any time t_k, the sum of the polynomials produced in the preceding section approximates the function. By netting of the spacial domain at any grid temporary point t_k and using the collocation method, the unknown coefficients of the series and parameter a are obtained. In the present method, at any grid temporary point t_k, the least square method is used for solving a nonlinear system. Finally, all points $(x_i, y_j, t_k, u(x_i, y_j, t_k))$ are interpolated using B-spline polynomials in domain Ω.

Time discretization

For discretization of $[0,T]$, consider

$$t_k = k\tau, \quad k = 0,1,2,\cdots,M,$$

where $\tau = \frac{T}{M}$. For discretization of the problems (1) and (2), we use the forward FDM:

$$\frac{u^{k+1}-u^k}{\tau} - \frac{u_{xx}^{k+1}+u_{xx}^k}{2} - \frac{u_{yy}^{k+1}+u_{yy}^k}{2} = r^k f^{k+\frac{1}{2}},$$

where $r^k = r(t_k)$ and $f^{k+\frac{1}{2}} = \frac{f^k + f^{k+1}}{2}$ and $u^{k+1} = u(X, Y, t_{k+1})$.

Simplified phrase will be:

$$2u^{k+1} - \tau(u_{xx}^{k+1} + u_{yy}^{k+1}) = 2u^k + \tau(u_{xx}^k + u_{yy}^k) + 2\tau r^k f^{k+\frac{1}{2}}, \quad k = 0,1,2,\cdots,M. \tag{12}$$

Problem 1)

After integrating of the Eq.(3), and using integral condition, the $r(t)$ is obtained:

$$r(t) = \frac{\int_0^1\int_0^1 u(x,y,t)dxdy}{E(t)}.$$

In addition to Eq.(12), we have for each t_k the following equations:

$$u^0 = \psi(x,y), \quad (x,y) \in [0,1]^2,$$
$$u^k(x,y) = \chi(x,y,t_k)r(t_k), \quad (x,y) \in [0,1]^2,$$
$$r^k = r(t_k) = \frac{\int_0^1\int_0^1 u(x,y,t_k)dxdy}{E(t_k)},$$

that we obtain a nonlinear equation system.

Problem 2)

According to Eq.(4), in addition Eq.(12), we have for each t_k:

$$u^0 = \psi(x,y), \quad (x,y) \in [0,1]^2,$$
$$u^k(x,y) = \chi(x,y,t_k)r(t_k), \quad (x,y) \in [0,1]^2,$$
$$r^k = r(t_k) = \frac{u(x_0, y_0, t_k)}{E(t_k)},$$

that we obtain a nonlinear equation system.

Implementation for the problems

Suppose u^{j+1} is written as follows:

$$u^{j+1} \cong \sum_{l=0}^{N}\sum_{m=0}^{N} c_{lm}^{j+1} A_l(x) A_m(y). \tag{13}$$

For the higher order derivatives of the above series w.r.t x and y, we have:

$$u_x^{j+1} \cong \sum_{l=0}^{N}\sum_{m=0}^{N} c_{lm}^{j+1} A_l'(x) A_m(y), \tag{14}$$

$$u_{xx}^{j+1} \cong \sum_{l=0}^{N}\sum_{m=0}^{N} c_{lm}^{j+1} A_l''(x) A_m(y), \tag{15}$$

$$u_y^{j+1} \cong \sum_{l=0}^{N}\sum_{m=0}^{N} c_{lm}^{j+1} A_l(x) A_m'(y), \tag{16}$$

$$u_{yy}^{j+1} \cong \sum_{l=0}^{N}\sum_{m=0}^{N} c_{lm}^{j+1} A_l(x) A_m''(y). \tag{17}$$

For each t_j, we put these equations in problems (1) and (2). By discretizing the domain $[0,1]^2$, a nonlinear system including a unknown parameter a and $(N+1)^2 + 1$ unknowns $c_{l,m}^{j+1},\quad l,m=0,1,2,\cdots,N$ with $(N+1)^2 + 1$ equations is obtained. To find a and $c_{l,m}^{j+1},\quad l,m=0,1,2,\cdots,N$, can be minimized L_2 norm of residual using least squares method.

For implementing the method, we will consider the following collocation grid points:

Regular grid points

$$x_k = c + \frac{d-c}{N}(k-1),\quad k = 1,2,\dots,N+1,\quad c \le x_k \le d.$$

Chebyshev-Gauss-Lobatto (CGL) grid points

$$x_k = c + \frac{d-c}{2}(1-\varsigma_k),\quad k = 0,1,\dots,N,\quad c \le x_k \le d,$$

where

$$\varsigma_k = \cos\left(\frac{k\pi}{N}\right),\quad k = 0,1,\dots,N,\quad -1 \le \varsigma_k \le 1.$$

Convergence and Stability Theorems

Suppose that $\Lambda = [-1,1]$ and $L_\omega^2(\Lambda)$ be function Hilbert space with the standard inner product

$$(f,g)_\omega = \int_{-1}^{1} \omega(t) f(t) g(t)\,dt,$$

where $\omega(t) = \sqrt{1-t^2}$ is positive weight function and $\|.\|_\omega^2 = (.,.)$. Let N be positive integer, we will consider the subspace of $L_\omega^2(\Lambda)$ by using the second kind of Chebyshev polynomials as

$$S_N = span\{U_0, U_1, \ldots, U_N\}.$$

We define $L_\omega^2(\Lambda)$ -orthogonal projection as follows:

$$P_N : L_\omega^2(\Lambda) \to S_N$$
$$(P_N v)(t) = \sum_{i=0}^{N} c_i U_i(t),$$

such that $(P_N v - v, \varphi)_\omega = 0,\ \forall \varphi \in S_N$. To estimate $\|P_N v - v\|_\omega$, we have the space interpolation:

$$H_{\omega,R}^r(\Lambda) = \left\{ v \,|\, v \text{ is measurable and } \|v\|_{r,\omega,R} < \infty \right\},$$

where $r > 0$ is any real number, and

$$\|v\|_{r,\omega,R} = \left(\sum_{i=0}^{r} \left\| (t+2)^{\frac{r}{2}+i} \frac{d^i v}{dt^i} \right\|_\omega^2 \right)^{1/2}. \tag{18}$$

We define the Sturm-Liouville operator of the second-kind Chebyshev polynomials, R, as

$$R(U_n(t)) = -\omega^{-1}(t)\frac{d}{dt}\left(\omega^3(t)\frac{d}{dt}U_n(t)\right), \tag{19}$$

see [20], Chapter 5.

Proposition 4.1: R_m is a continuous mapping from $H_{\omega,R}^{2m}(\Lambda)$ to $L_\omega^2(\Lambda)$.

Proof: For showing this, we will prove that

$$R^m v(t) = \sum_{k=1}^{2m} (t+2)^{m+k} q_k(t) \frac{d^k v(t)}{dt^k}, \tag{20}$$

where q_k is a rational bounded uniformly function on the whole interval Λ. It is proved by induction. For $m = 1$, we have

$$Rv(t) = 3t\frac{dv}{dt} - (1-t^2)\frac{d^2 v}{dt^2}$$
$$= (t+2)^2\left(\frac{3t}{(t+2)^2}\right)\frac{dv}{dt} + (t+2)^3\left(\frac{t-1}{(t+2)^2}\right)\frac{d^2 v}{dt^2}.$$

Suppose that for m, n the relation (20) is satisfied. One can easily prove that this relation is established for $m = n + 1$.

Proposition 4.2: For any real $r \ge 0$, $v \in H_{\omega,R}^r(\Lambda)$, $v = \sum_{n=0}^{\infty} \hat{v}_n U_n(t)$ then

$$\|P_N v - v\|_\omega \le cN^{-r} \|v\|_{r,\omega,R}, \qquad (21)$$

for some real constant c.

Proof: First, we suppose that $r = 2m$. Due to the (7), (8), (19) and integration by parts,

$$\begin{aligned}
\hat{v}_n &= \frac{2}{\pi}\int_\Lambda v(t)U_n(t)\omega(t)dt = \frac{2}{\pi n(n+2)}\int_\Lambda v(t)RU_n(t)\omega(t)d\eta \\
&= -\frac{2}{\pi n(n+2)}\int_\Lambda v(t)\frac{d}{dt}(\omega^3(t)\frac{d}{dt}U_n(t))dt \\
&= \frac{2}{\pi n(n+2)}\int_\Lambda \omega^3(t)\frac{d}{dt}v(t)(\frac{d}{dt}U_n(t))dt \\
&= -\frac{2}{\pi n(n+2)}\int_\Lambda \frac{d}{dt}(\omega^3(t)\frac{d}{dt}v(t))U_n(t)dt \\
&= \frac{2}{\pi n(n+2)}\int_\Lambda Rv(t)U_n(t)\omega(t)dt \\
&= \ldots = \frac{2}{\pi n^m(n+2)^m}\int_\Lambda R^m v(t)U_n(t)\omega(t)dt.
\end{aligned} \qquad (22)$$

Now according to (20), (22) and definition of $H^{2m}_{\omega,R}(\Lambda)$, we have:

$$\| P_N v - v \|^2_\omega = \sum_{n=N+1}^{\infty} (\hat{v}_n)^2 \| U_n \|^2_\omega \le cN^{-4m} \| v \|^2_{r,\omega,R}.$$

Next, we put $r = 2m + 1$. By (10), (7) and integration by part, we have:

$$\begin{aligned}
\hat{v}_n &= \frac{2}{\pi n^m(n+2)^m}\int_\Lambda R^m v(t)U_n(t)\omega(t)dt \\
&= -\frac{2}{\pi n^{m+1}(n+2)^{m+1}}\int_\Lambda R^m v(t)\frac{d}{dt}(\omega^3(t)\frac{d}{dt}U_n(t))dt \\
&= -\frac{2}{\pi n^{m+1}(n+2)^{m+1}}\int_\Lambda \frac{d}{dt}(R^m v(t))\frac{d}{dt}U_n(t)\omega^3(t)dt.
\end{aligned}$$

Now using (9) and (20), we complete the proof.

The general result follows from the previous results and space interpolation.

Theorem 4.1: For any real $r > 0$, $y \in H^r_{\omega,R}(\Lambda)$, we have:

$$\| y_N - y \|_\omega \le c(N-2)^{-r} \| y \|_{r,\omega,R},$$

for some constant c.

Proof: Using Eq. (6) and Proposition(4.2), we get the proof.

The Chebyshev–Gauss interpolation operator $I_N f(t) : C(\bar{\Lambda}) \to R_N$ is

$$I_N f(\varsigma_{N,j}) = f(\varsigma_{N,j}), \qquad 0 \le j \le N,$$

that $\varsigma_{N,j} = \cos(2j\pi/(2N+1))$ are the $N+1$ Chebyshev-Gauss points. The following theorem is related to the stability of the Chebyshev–Gauss interpolation.

Theorem 4.2: For any $f \in H^1_{\omega,R}$, $\exists c \in \mathbb{R}$ such that

$$\| I_N f \|_{L^2(\Lambda)} \le c\left(\| f \|_{L^2(\Lambda)} + N^{-1} \| f \|_{H^1_{\omega,R}(\Lambda)}\right).$$

Proof: See [20].

This theorem shows that the a-polynomial approximation has exponential convergence. The ssimilar theorems which have been proved in this section can be seen in [21] for the Chebyshev polynomials of the first kind.

Numerical Examples

Example 1

Assume problem (1) with:

$$\begin{gathered}
\psi(x,y,t) = (\frac{5\pi^2}{16} - 5t)e^t \sin(\frac{\pi}{4}(x+2y)), \\
k_0(0,y,t) = e^t \sin(\frac{\pi y}{2}), \\
k_1(1,y,t) = e^t \sin(\frac{\pi}{4}(1+2y)), \\
l_0(x,0,t) = e^t \sin(\frac{\pi x}{4}), \\
l_1(x,1,t) = e^t \sin(\frac{\pi}{4}(x+2)), \\
E(t) = \frac{8}{\pi^2}e^t, \\
f(x,y) = \sin(\frac{\pi}{4}(x+2y)).
\end{gathered}$$

The exact solution is given by:

$$\{w(x,y,t), P(t)\} = \left\{e^t \sin(\frac{\pi}{4}(x+2y)), 1+5t\right\}.$$

This example is estimated with regular and CGL grid points. Absolute errors at some nodal points are given in Tables 1-4. The absolute errors are also listed in the tables by introducing artificial error 10^{-2} into the right end and initial condition. In Tables 1 and 2, CGL and regular grid points are used, respectively, and the absolute errors of $P(t)$ obtained by the present method are compared with the (1,9) FTCS method [12]. In Tables 3 and 4, regular and CGL grid points are used, respectively, and the absolute errors of $u(x, y)$ (see Eq.(3) for the definition) obtained by the present method are compared with the (1,9) FTCS method [12] at $T = 1$. The results of the present method in with and without noise modes are more accurate than the (1,9) FTCS method [12]. In Figure 1, the exact and numerical solutions $P(t)$ are shown in two moods, with and without noise and at CGL grid points. In Figure 2, level curves of the absolute errors of $u(x, y)$ are shown in two cases, with and without noise at CGL grid points and $T = 1$. It can be seen from Figure 1(b) and Figure 2(b) the stability. In Figure 3 and Figure 4, graphs of $u(x, y)$ are shown for $N = 5$ and $\tau = 0.0005$ in CGL grid points at $T = 1$, with and without noise.

Table 1. Example 1, the absolute errors of $P(t)$
$N = 5$, $\tau = 0.0005$, $T = 1$ and CGL points

t	(1,9) FTCS [12]	Present method	Present method with noise
0.1	7.8e-04	1.63775e-04	2.47881e-02
0.2	7.6e-04	4.92752e-05	4.31753e-03
0.3	7.5e-04	1.39452e-05	7.88542e-04
0.4	7.3e-04	6.91637e-05	2.05503e-04
0.5	7.0e-04	6.89632e-05	1.24470e-04
0.6	6.9e-04	1.63994e-04	1.74604e-04
0.7	6.5e-04	2.31303e-04	2.33300e-04
0.8	6.7e-04	2.92222e-04	2.92603e-04
0.9	6.9e-04	3.52198e-04	3.52272e-04
1.0	6.5e-04	4.13071e-04	4.13085e-04

Table 2. Example 1, the absolute errors of $P(t)$
$N = 5$, $\tau = 0.0005$, $T = 1$ and Regular grid points

t	(1,9) FTCS [12]	Present method	Present method with noise
0.1	7.8e-04	6.74683e-05	2.52819e-02
0.2	7.6e-04	1.69208e-05	4.35818e-03
0.3	7.5e-04	2.10545e-05	7.95207e-04
0.4	7.3e-04	6.80101e-05	2.06179e-04
0.5	7.0e-04	1.21761e-04	1.46781e-04
0.6	6.9e-04	1.77630e-04	1.82226e-04
0.7	6.5e-04	2.34915e-04	2.35771e-04
0.8	6.7e-04	2.93410e-04	2.93572e-04
0.9	6.9e-04	3.53126e-04	3.53157e-04
1.0	6.5e-04	4.14122e-04	4.14129e-04

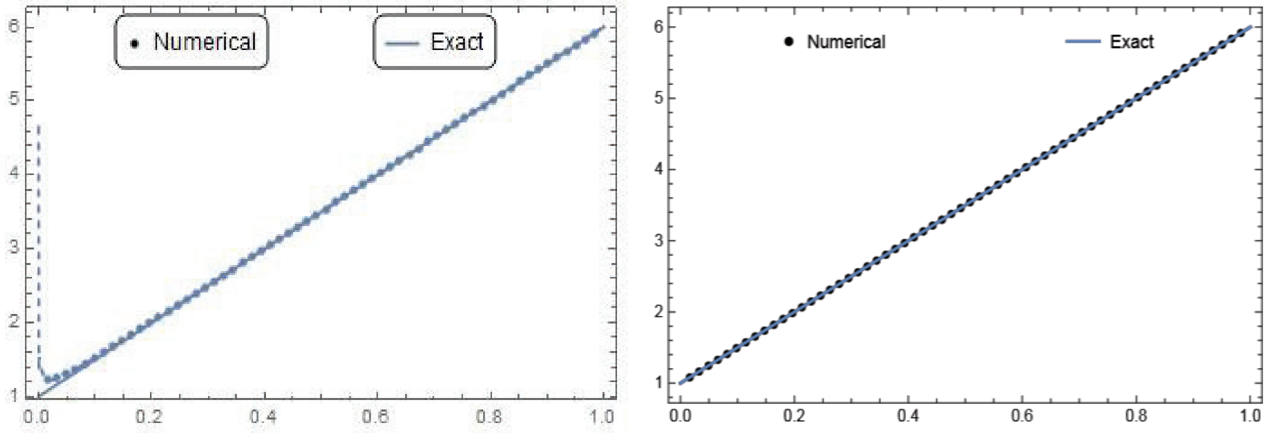

(a) (b)

Figure 1. Graphs of the exact and numerical solutions of $P(t)$ in Example 1 for $N = 5$ and $\tau = 0.0005$ in CGL grid points: (a) with noisy data; (b) without noisy data.

Table 3. Example 1, the absolute errors of $u(x, y)$
$N = 5$, $\tau = 0.0005$, $T = 1$ and CGL points

x	y	(1,9) FTCS [12]	Present method	Present method with noise
0.1	0.1	3.8e-04	1.87343e-06	1.87344e-06
0.2	0.2	3.6e-04	4.11858e-06	4.11852e-06
0.3	0.3	3.5e-04	9.80984e-06	9.80974e-06
0.4	0.4	3.4e-04	9.97414e-06	9.97400e-06
0.5	0.5	3.3e-04	1.37279e-05	1.37278e-05
0.6	0.6	3.2e-04	1.98700e-05	1.98698e-05
0.7	0.7	3.7e-04	1.76888e-05	1.76887e-05
0.8	0.8	3.2e-04	8.28951e-06	8.28946e-06
0.9	0.9	3.0e-04	3.59068e-06	3.59066e-06

Table 4. Example 1, the absolute errors of of $u(x, y)$
$N = 5$, $\tau = 0.0005$, $T = 1$ and Regular points

x	y	(1,9) FTCS [12]	Present method	Present method with noise
0.1	0.1	3.8e-04	5.34879e-06	5.34879e-06
0.2	0.2	3.6e-04	2.19912e-06	2.19910e-06
0.3	0.3	3.5e-04	1.19730e-05	1.19729e-05
0.4	0.4	3.4e-04	1.53551e-05	1.53551e-05
0.5	0.5	3.3e-04	1.79834e-05	1.79833e-05
0.6	0.6	3.2e-04	1.92278e-05	1.92277e-05
0.7	0.7	3.7e-04	1.54533e-05	1.54532e-05
0.8	0.8	3.2e-04	1.35557e-05	1.35557e-05
0.9	0.9	3.0e-04	1.46026e-05	1.46026e-05

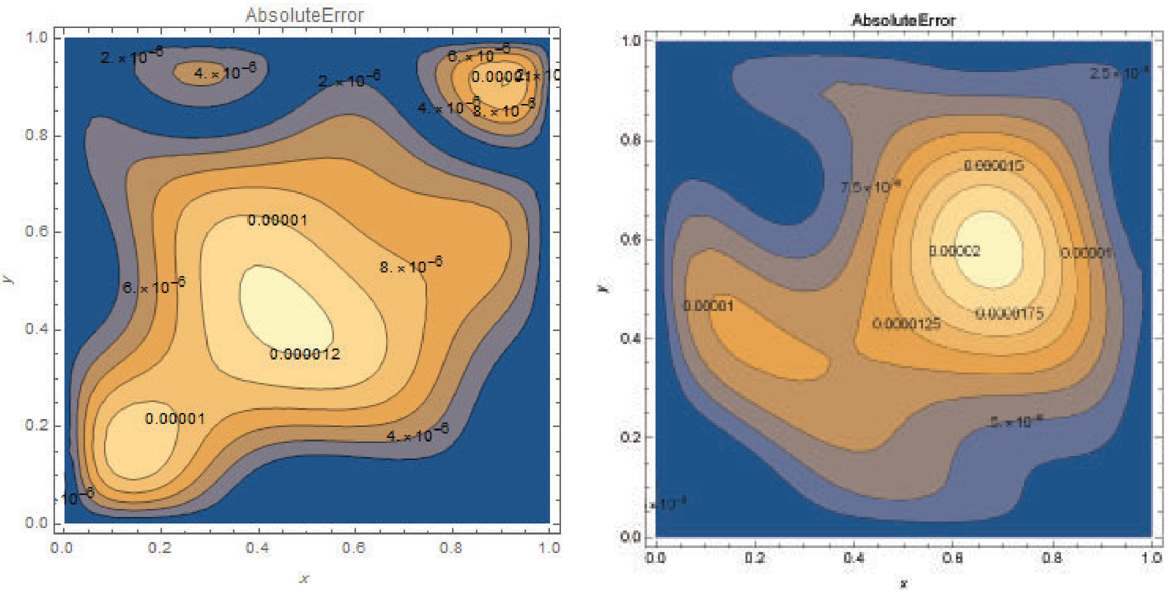

(a) **(b)**

Figure 2. Graphs of level curves of the absolute errors for $u(x, y)$ in Example 1 for of $N = 5$ and $\tau = 0.0005$, in CGL grid points at $T = 1$: (a) with noisy data; (b) without noisy data.

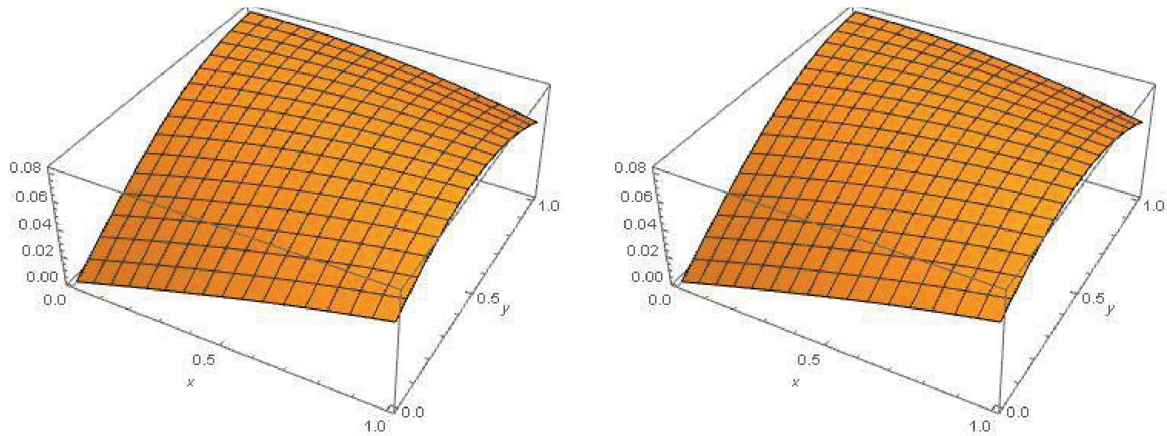

(a) **(b)**

Figure 3. Graphs of $u(x, y)$ in Example 1 for $N = 5$ and $\tau = 0.0005$ in CGL grid points at $T = 1$: (a) numerical solution; (b) exact solution.

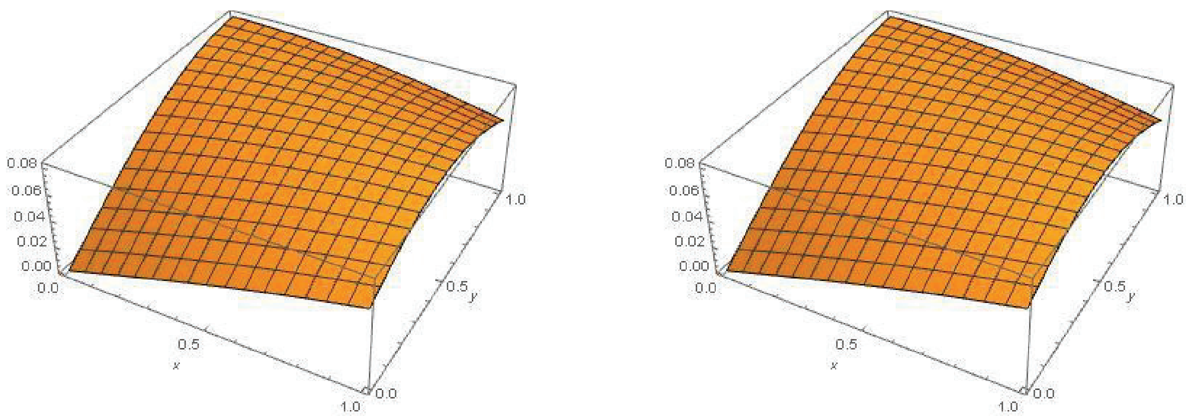

(a) **(b)**

Figure 4. Graphs of numerical solution $u(x, y)$ in Example 1 for $N = 5$ and $\tau = 0.0005$ in CGL grid points at $T = 1$: (a) with noisy data, (b) without noisy data.

Example 2

Assume problem (2) with:

$$\psi(x,y,t)=(\frac{5\pi^2}{16}-5t)e^t\sin(\frac{\pi}{4}(x+2y)),$$

$$k_0(0,y,t)=e^t\sin(\frac{\pi y}{2}),$$

$$k_1(1,y,t)=e^t\sin(\frac{\pi}{4}(1+2y)),$$

$$l_0(x,0,t)=e^t\sin(\frac{\pi x}{4}),$$

$$l_1(x,1,t)=e^t\sin(\frac{\pi}{4}(x+2)),$$

$$E(t)=e^t\sin(0.2\pi),$$

$$f(x,y)=\sin(\frac{\pi}{4}(x+2y)).$$

The exact solution is given by:

$$\{w(x,y,t),P(t)\}=\left\{e^t\sin(\frac{\pi}{4}(x+2y)),1+5t\right\}.$$

This example is estimated by regular and CGL grid points. Absolute errors at some nodal points are given in Tables 5-8. The absolute errors are also listed in the tables by introducing artificial error 10^{-2} into the right end and initial condition. In Tables 5 and 6, CGL and regular grid points are used, respectively, and the absolute errors of $P(t)$ achieved by the present method are compared with the (9,9) fully implicit method [11]. In Tables 7 and 8, CGL and regular grid points are used, respectively, and the absolute errors of $u(x, y)$ in Eq. (3) obtained by the present method are compared with the (9,9) fully implicit method [11] at $T = 1$. The results of the present method in with and without noise modes are more accurate than the (9,9) fully implicit method [11]. In Figure 5, the exact and numerical solutions $P(t)$ are shown in two moods, with and without noise and at CGL grid points. In Figure 4, level curves of the absolute errors of $u(x, y)$ are shown in two cases, with and without noise at $T = 1$ and CGL grid points. It can be seen from Figure 4(b) and Figure 5(b) that the present method is stable. In Figure 7 and Figure 8, graphs of $u(x, y)$ are shown for $N = 5$ and $\tau = 0.0002$ in CGL grid points at $T = 1$, with and without noise.

Table 5. Example 2, the absolute errors of $P(t)$ $N = 5$, $\tau = 0.0002$, $T = 1$ and CGL points

t	(9,9) Fully implicit [11]	Present method	Present method with noise
0.1	2.1e-05	1.46409e-04	4.92584e-02
0.2	2.3e-05	3.47002e-05	1.00857e-02
0.3	2.4e-05	1.76180e-05	2.06723-e03
0.4	2.5e-05	5.71086e-05	4.66622e-04
0.5	2.6e-05	9.36641e-05	1.74350e-04
0.6	2.6e-05	1.29301e-04	1.44968e-04
0.7	2.4e-05	1.64419e-04	1.67415e-04
0.8	2.3e-05	1.99088e-04	1.99652e-04
0.9	2.3e-05	2.33313e-04	2.33417e-04
1.0	2.2e-05	2.67086e-04	2.67105e-04

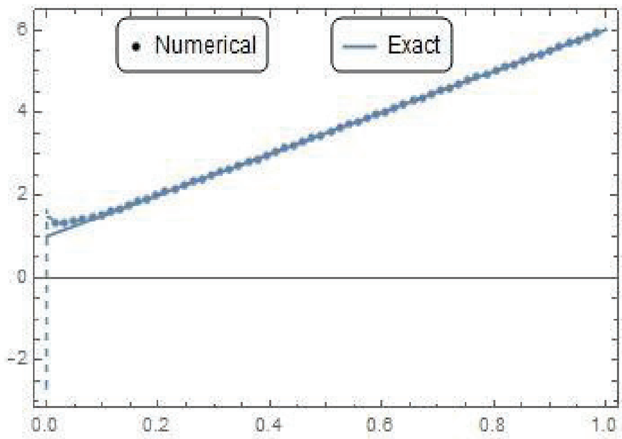

(a)

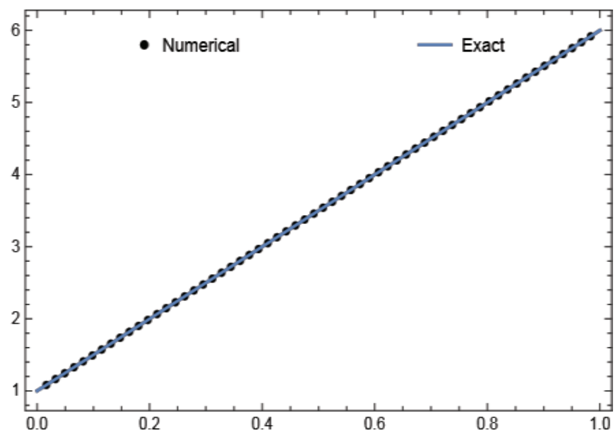

(b)

Figure 5. Graphs of the exact and numerical solutions of $P(t)$ in Example 2 for $N = 5$, $\tau = 0.0002$ in CGL grid points: (a) with noisy data; (b) without noisy data.

Table 6. Example 2, the absolute errors of $P(t)$
$N = 5$, $\tau = 0.0002$, $T = 1$ and Regular grid points

t	(9,9) Fully implicit [11]	Present method	Present method with noise
0.1	2.1e-05	8.79941e-05	5.02518e-02
0.2	2.3e-05	2.93465e-06	1.02132e-02
0.3	2.4e-05	7.60471e-06	2.06522-e03
0.4	2.5e-05	3.86712e-05	4.47073e-04
0.5	2.6e-05	7.35956e-05	1.53445e-04
0.6	2.6e-05	1.08973e-04	1.24341e-04
0.7	2.4e-05	1.44109e-04	1.47018e-04
0.8	2.3e-05	1.78853e-04	1.79394e-04
0.9	2.3e-05	2.13163e-04	2.13262e-04
1.0	2.2e-05	2.47019e-04	2.47036e-04

Table 7. Example 2, the absolute errors of $u(x, y)$
$N = 5$, $\tau = 0.0002$, $T = 1$ and CGL points

x	y	(9,9) FTCS [11]	Present method	Present method with noise
0.1	0.1	7.5e-06	2.32376e-07	2.32367e-07
0.2	0.2	7.4e-06	6.93914e-07	6.93881e-07
0.3	0.3	7.5e-06	3.11295e-06	3.11289e-06
0.4	0.4	7.8e-06	6.16557e-06	6.16549e-06
0.5	0.5	7.9e-06	7.75301e-06	7.75292e-06
0.6	0.6	7.6e-06	6.72182e-06	6.72174e-06
0.7	0.7	7.8e-06	3.76836e-06	3.76830e-06
0.8	0.8	7.7e-06	1.09950e-06	1.09947e-06
0.9	0.9	8.0e-06	5.51475e-07	5.51468e-07

Table 8. Example 2, the absolute errors of $u(x, y)$
$N = 5$, $\tau = 0.0002$, $T = 1$ and Regular points

x	y	(9,9) FTCS [11]	Present method	Present method with noise
0.1	0.1	7.5e-06	2.97402e-06	2.97401e-06
0.2	0.2	7.4e-06	4.56481e-06	4.56478e-06
0.3	0.3	7.5e-06	6.09955e-06	6.09949e-06
0.4	0.4	7.8e-06	7.74896e-06	7.74888e-06
0.5	0.5	7.9e-06	8.70313e-06	8.70304e-06
0.6	0.6	7.6e-06	8.38167e-06	8.38159e-06
0.7	0.7	7.8e-06	7.18318e-06	7.18313e-06
0.8	0.8	7.7e-06	5.92508e-06	5.92505e-06
0.9	0.9	8.0e-06	4.29058e-06	4.29057e-06

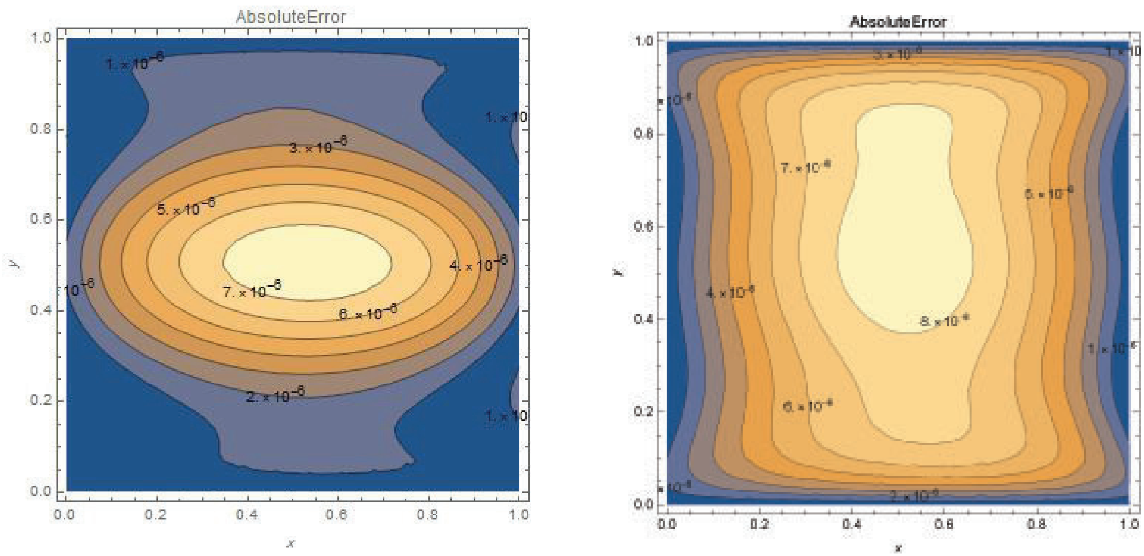

(a) (b)

Figure 6. Graphs of level curves of the absolute errors for $u(x, y)$ in Example 2 for $N = 5$, $\tau = 0.0002$ in CGL grid points at $T = 1$: (a) with noisy data, (b) without noisy data.

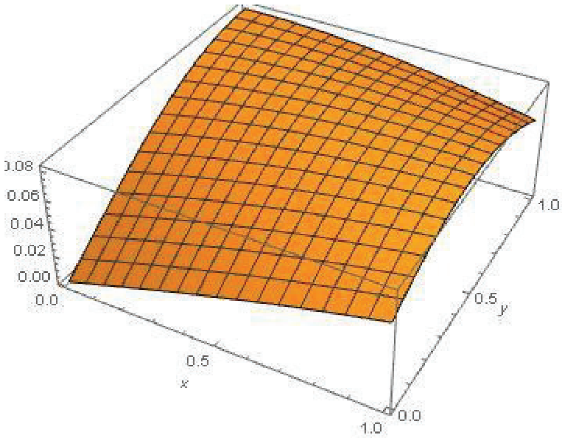

(a)

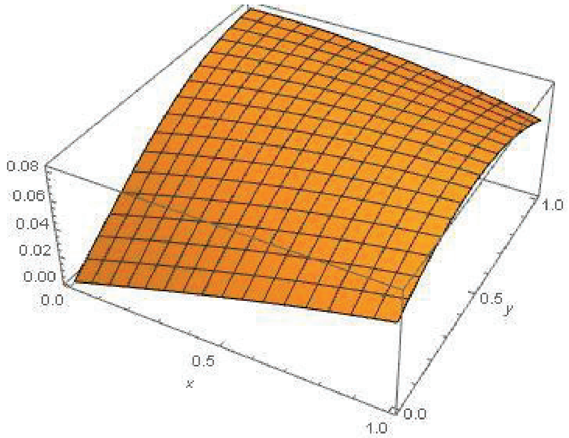

(b)

Figure 7. Graphs of $u(x, y)$ in Example 2 for $N = 5$, $\tau = 0.0002$ in CGL grid points at $T = 1$: (a) numerical solution; (b) exact solution.

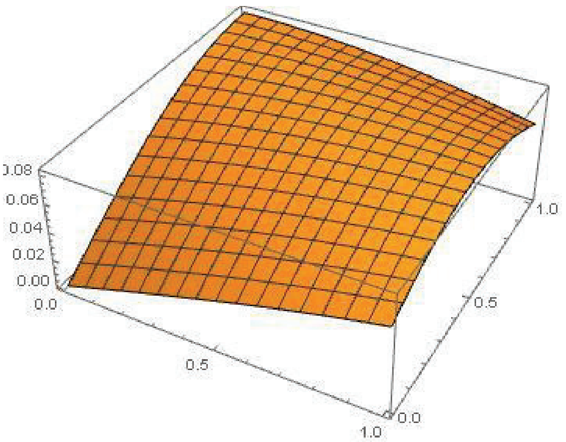

(a)

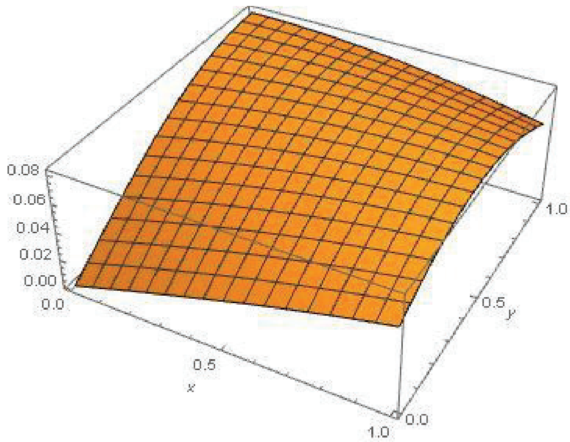

(b)

Figure 8. Graphs of numerical solution $u(x, y)$ in Example 2 for $N = 5$, $\tau = 0.0002$ in CGL grid points at $T = 1$: (a) with noisy data; (b) without noisy data.

CONCLUSION

Here, we have successfully implemented a new method to solve two-dimensional parabolic inverse problems. The problems have nonlocal boundary conditions. Comparing the results of the present method and the results of previous papers, the present method yields better results. The present method is easy to consider boundary conditions and is convergence and stable with respect to noise. According to the previous section tables, it is observed that the present method is stable and its results are better than finite difference method.

AUTHORSHIP CONTRIBUTIONS

Authors equally contributed to this work.

DATA AVAILABILITY STATEMENT

The authors confirm that the data that supports the findings of this study are available within the article. Raw data that support the finding of this study are available from the corresponding author, upon reasonable request.

CONFLICT OF INTEREST

The author declared no potential conflicts of interest with respect to the research, authorship, and/or publication of this article.

ETHICS

There are no ethical issues with the publication of this manuscript.

REFERENCES

[1] Linde N, Renard P, Mukerji T, Caers J. Geological realism in hydrogeological and geophysical inverse modeling: A review. Adv Water Res 2015;86:86−101. [CrossRef]
[2] Bal G, Schotland JC. Inverse scattering and acousto-optic imaging. Phys Rev Lett 2010;104:043902. [CrossRef]
[3] Baraniuk R, Steeghs P. Compressive radar imaging. 2007 IEEE Radar Conference; 2007 Apr 17-20; Waltham, USA: IEEE; 2007. pp. 128−133. [CrossRef]
[4] Isakov V, Wu SF. On theory and application of the Helmholtz equation least squares method in inverse acoustics. Inverse Probl 2002;18:1147. [CrossRef]
[5] Widrow B, Walach E. Adaptive inverse control, reissue edition: A signal processing approach. New York: Wiley; 2014.
[6] Crossen E, Gockenbach MS, Jadamba B, Khan AA, Winkler B. An equation error approach for the elasticity imaging inverse problem for predicting tumor location. Comput Math Appl 2014;67:122−135. [CrossRef]
[7] Yousefi SA. Finding a control parameter in a one-dimensional parabolic inverse problem by using the Bernstein Galerkin method. Inverse Probl Science Eng 2009;17:821−828. [CrossRef]
[8] Dehghan M. Parameter determination in a partial differential equation from the overspecified data. Math Comput Model 2005;41:196−213. [CrossRef]
[9] Lerma A, Hinestroza D. Coefficient identification in the Euler-Bernoulli equation using regularization methods. Appl Math Model 2017;41:223−235. [CrossRef]
[10] Dehghan M, Tatari M. Determination of a control parameter in a one-dimensional parabolic equation using the method of radial basis functions. Math Comput Model 2006;44:1160−1168. [CrossRef]
[11] Dehghan M. Fourth-order techniques for identifying a control parameter in the parabolic equations. Int J Eng Sci 2002;40:433−447. [CrossRef]
[12] Dehghan M. Numerical methods for two-dimensional parabolic inverse problem with energy overspecification. Int J Comput Math 2001;77:441−455. [CrossRef]
[13] Hajishafieiha J, Abbasbandy S. A new method based on polynomials equipped with a parameter to solve two parabolic inverse problems with a nonlocal boundary condition. Inverse Probl Sci Eng 2020;28:739−753. [CrossRef]
[14] Cui MG, Lin YZ, Yang LH. A new method of solving the coefficient inverse problem. Sci China Math 2007;50:561−572. [CrossRef]
[15] Cannon JR, Lin Y, Wang S. Determination of source parameter in parabolic equations. Meccanica 1992;27:85−94. [CrossRef]
[16] Ellahi R, Hameed, M. Numerical analysis of steady non-Newtonian flows with heat transfer analysis, MHD and nonlinear slip effects. Int J Numer Method Heat Fluid Flow 2012;22:24−38. [CrossRef]
[17] Ellahi R, Wang X, Hameed M. Effects of heat transfer and nonlinear slip on the steady flow of Couette fluid by means of Chebyshev spectral method. Z Naturforsch 2014;69:1−8. [CrossRef]
[18] Abbasbandy S. A new class of polynomial functions equipped with a parameter. Math Sci 2017;11:127−130. [CrossRef]
[19] Hajishafieiha J, Abbasbandy S. A new class of polynomial functions for approximate solution of generalized Benjamin-Bona-Mahony-Burgers (gBBMB) equations. Appl Math Comput 2020;367:124765. [CrossRef]
[20] Bernardi C, Maday Y. Spectral methods. Handb Numer Anal 1997;5:209−485. [CrossRef]
[21] Guo BY, Shen J, Wang ZQ. Chebyshev rational spectral and pseudospectral methods on a semi-infinite interval. Int J Numer Methods Eng 2002;53:65−84. [CrossRef]
[22] Gulnaz O, Kaya A, Dincer S. The reuse of dried activated sludge for adsorption of reactive dye. J Hazard Mater 2006;134:190−196. [CrossRef]
[23] Jain AK, Gupta VK, Bhatnagar A, Suhas A. Utilization of industrial waste products as adsorbents for the removal of dyes. J Hazard Mater 2003;101:31−42. [CrossRef]
[24] Mohan SV, Ramanaıah SV, Sarma PN. Biosorption of direct azo dye from aqueous phase onto Spirogyra sp. I02: Evaluation of kinetics and mechanistic aspect. Biochem Eng J 2008;38:61−69. [CrossRef]
[25] Ozcan A, Oncu EM, Ozcan AS. Kinetics isotherm and thermodynamic studies of adsorption of acid blue 193 from aqueous solutions onto natural sepiolite. Colloid Surf A 2006;277:90−97. [CrossRef]
[26] Aksu Z, Tezer S. Equilibrium and kinetic modelling of biosorption of Remazol Black B by Rhizopus arrhizus in a batch system: effect of temperature. Process Biochem 2000;36:431−439. [CrossRef]
[27] Ince NH, Tezcanlı G. Reactive dyestuff degradation by combined sonolysis and ozonation. Dyes Pigm 2001;49:145−153. [CrossRef]
[28] Xubiao L, Youcai Z, Yining H, Lixia Y, Xinman T, Shenglian L. Removal of water-soluble acid dyes from water environment using a novel magnetic molecularly imprinted polymer. J Hazard Mater 2011;187:274−282. [CrossRef]
[29] Behnamfard A, Salarirad MM. Equilibrium and kinetic studies on free cyanide adsorption from aqueous solution by activated carbon. J Hazard Mater 2009;170:127−133. [CrossRef]

[30] Bhattacharyya K. Adsorption characteristics of the dye, Brilliant Green, on Neem leaf powder. Dyes Pigm 2003;57:211−222. [CrossRef]

[31] Crini G. Non-conventional low-cost adsorbents for dye removal: A review. Bioresour Technol 2006;97:1061−1085. [CrossRef]

[32] Mohan D, Pittman CU. Activated carbons and low cost adsorbents for remediation of tri- and hexavalentchromium from water. J Hazard Mater 2006;137:762−811. [CrossRef]

[33] Ahmad AL, Loh MM, Aziz JA. Preparation and characterization of activated carbon fromoil palm wood and its evaluation on methylene blue adsorption. Dyes Pigm 2007;75:263−272. [CrossRef]

[34] Suteu D, Biliuta G, Rusu L, Coseri S, Nacu G. Cellulose cellets as new type of Adsorbent for the removal of Dyes from aqueous media. Environ Eng Manag J 2015;14:525−532. [CrossRef]

[35] Calvete T, Lıma EC, Cardoso NF, Dıas SLP, Pavan FA. Application of carbon adsorbents prepared from the Brazilian pine-fruit-shell for the removal of procion red MX 3B from aqueous solution-kinetic, equilibrium, and thermodynamic studies. Chem Eng J 2009;155:627−636. [CrossRef]

[36] ELwakeel KZ, Atia AA. Uptake of U(VI) from aqueous media by magnetic Schiff's base chitosan composite. J Cleaner Prod 2014;70:292−302. [CrossRef]

[37] ELwakeel KZ, Atia AA, Guibal E. Removal of uranium from aqueous medium using tetraethylenepentamine modifed magnetic chitosan resin. Bioresour Technol 2014;160:107−114. [CrossRef]

[38] Kemshead JT, Ugelstad J. Magnetic separation techniques: Their application to medicine. J Mol Cell Biochem 1985;67:11−18. [CrossRef]

[39] Monier M, Ayad DM, Wei Y, Sarhan AA. Adsorption of Cu(II), Co(II), and Ni(II) ions by modified magnetic chi-tosan chelating resin. J Hazard Mater 2010;177:962−970. [CrossRef]

[40] Ozay O, Ekici S, Baran Y, Aktas N, Sahiner N. Removal of toxic metal ions with magnetic hydrogels. Water Research 2009;43:4403−4411. [CrossRef]

[41] Hua M, Zhang S, Pan B, Zhang W, Zhang L, Lv Q. Heavy metal removal from water/wastewater by nanosized metal oxides: A review. J Hazard Mater 2011;211-212:317−331. [CrossRef]

[42] Mahdavian AR, Mirrahim MAS. Efficient separation of heavy metal cations by anchoring polyacrylic acid n superparamagnetic magnetite nanoparticles through surface modification. Chem Eng J 2010;159:264−271. [CrossRef]

[43] Wang XS, Ren JJ, Lu HJ, Zhu L, Liu F, Zhang Q, et al. Removal of Ni(II) from aqueous solutions by nanoscale magnetite. Clean Soil Air Water 2010;38:1131−1136. [CrossRef]

[44] Yang K, Xu NS, Su WW. Co-immobilized enzymes in magnetic chitosan beads for improved hydrolysis of macromolecular substrates under a time-varying magnetic field. J Biotechnol 2010;148:119. [CrossRef]

[45] Kinoshita T, Seino S, Mizukoshi Y, Nakagawa T, Yamamoto TA. Radiochemical synthesis of Au/Iron-oxide composite nanoparticles using PEG. J Magn Magn Mater 20007;311:255.

[46] Pimpha N, Chaleawlert-umpon S, Chruewkamlow N, Kasinrerk W. Preparation of anti-CD4 monoclonal antibody-conjugated magnetic poly(glycidyl methacrylate) particles and their application on CD4+ lymphocyte separation. Talanta 2011;84:89−97. [CrossRef]

[47] Liu ZL, Ding ZH, Yao KL, Tao J, Du GH, Lu QH, et al. Preparation and characterization of polymer-coated core-shell structured magnetic microbeads. J Magn Magn Mater 2003;265:98−105. [CrossRef]

[48] Liu X, Liu H, Xing J, Guan Y, Ma Z, Shan G, et al. Preparation and characterization of superparamagnetic functional polymeric microparticles. China Particuol 2003;1:76−79. [CrossRef]

[49] Yuwei C, Jianlong W. Preparation and characterization of magnetic chitosan nanoparticles and its application for Cu(II) removal. Chem Eng J 2011;168:286−292. [CrossRef]

[50] Yang ZG, Tang L, Lei X, Zeng G, Cai Y, Wei X, et al. Cd(II) removal from aqueous solution by adsorption on _-ketoglutaric acid-modified magnetic chitosan. Appl Surf Sci 2014;292:710−716. [CrossRef]

[51] Leechart P, Nakbanpote W, Thıravetyan P. Application of 'waste' wood-shaving bottom ash for adsorption of azo reactive dye. J Environ Manag 2008;90:912−920. [CrossRef]

[52] Senel S, Uzun L, Kara A, Denizli A. Heavy metal removal from synthetic solutions with magnetic beads under magnetic field. J Macromol Sci P App Chem 2008;45:635−642. [CrossRef]

[53] Kara A, Demirbel E. Kinetic, ısotherm and thermodynamic analysis on adsorption of Cr(VI) ıons from aqueous solutions by synthesis and characterization of magnetic-poly (divinylbenzene-vinylimidazole) microbeads. Water Air Soil Pollut 2012;223:2387−2403. [CrossRef]